A Comparative Study of Phosphoric Acid-Doped *m*-PBI Membranes

Kelly A. Perry,[1] Karren L. More,[1] E. Andrew Payzant,[2] Roberta A. Meisner,[3] Bobby G. Sumpter,[4] Brian C. Benicewicz[5]

[1]Oak Ridge National Laboratory, Materials Science and Technology Division, 1 Bethel Valley RD, Oak Ridge, Tennessee
[2]Oak Ridge National Laboratory, Chemical & Engineering Materials Division, Oak Ridge, Tennessee
[3]University of Tennessee, Materials Science and Engineering, Knoxville, Tennessee
[4]Oak Ridge National Laboratory, Computer Science & Mathematics Division and Center for Nanophase Materials Sciences, Oak Ridge, Tennessee
[5]University of South Carolina, Department of Chemistry and Biochemistry & USC NanoCenter, Columbia, South Carolina
Correspondence to: K. A. Perry (E-mail: perryka@ornl.gov)

Received 4 September 2013; revised 8 October 2013; accepted 9 October 2013; published online 31 October 2013
DOI: 10.1002/polb.23403

ABSTRACT: Phosphoric acid (PA)-doped *m*-polybenzimidazole (PBI) membranes used in high temperature fuel cells and hydrogen pumps were prepared by a conventional imbibing process and a sol–gel fabrication process. A comparative study was conducted to investigate the critical properties of PA doping levels, ionic conductivities, mechanical properties, and molecular ordering. This systematic study found that sol–gel PA-doped *m*-PBI membranes were able to absorb higher acid doping levels and to achieve higher ionic conductivities than conventionally imbibed membranes when treated in an equivalent manner. Even at similar acid loadings, the sol–gel membranes exhibited higher ionic conductivities. Heat treatment of conventionally imbibed membranes with $\leq$29 wt % solids caused a significant reduction in mechanical properties; conversely, sol–gel membranes exhibited an enhancement in mechanical properties. From X-ray structural studies and atomistic simulations, both conventionally imbibed and sol–gel membranes exhibited *d*-spacings of 3.5 and 4.6 Å, which were tentatively attributed to parallel ring stacking and staggered side-to-side packing, respectively, of the imidazole rings in these aromatic heterocyclic polymers. An anisotropic staggered side-to-side chain packing present in the conventional membranes may be related to the reduction in mechanical properties. 2013 Wiley Periodicals, Inc.† J. Polym. Sci., Part B: Polym. Phys. **2014**, *52*, 26–35

KEYWORDS: conducting polymers; fuel cells; high temperature; ionomers; membranes; phosphoric acid-doped polybenzimidazole; proton exchange membrane; WAXS

INTRODUCTION Fuel cells are electrochemical energy conversion devices that convert chemical energy directly into electrical energy in an efficient manner. A critical component of these electrochemical devices and where the chemical conversion of hydrogen to electricity takes place is the membrane electrode assembly (MEA). The MEA is composed of a proton exchange membrane (PEM) sandwiched between two porous catalyst/electrode layers. For the commercial viability of fuel cells, the PEM must have rapid ionic transport while maintaining mechanical integrity and long-term durability. Related devices, such as electrochemical hydrogen pumps, rely on membranes with similar properties for their efficient operation.[1] A PEM that addresses these important challenges is phosphoric acid (PA)-doped polybenzimidazole (PBI).[2–4]

Much research has focused on the well-characterized perfluorosulfonic acid (PFSA)-based PEMs. Such membranes use water as the medium to transport protons and are believed to transport protons mainly through a vehicular mechanism, although at low relative humidity there may be structural Grotthuss diffusion.[5] The PFSA-based fuel cells with water as the electrolyte are generally limited to operating at temperatures less than 100 °C and are most commonly operated at 80 °C with 100% humidified gas feed streams.[6]

PEM fuel cell operation at temperatures higher than 100 °C and under anhydrous feed streams has many advantages. High temperatures permit faster electrochemical reactions on the noble metal catalyst, which is especially beneficial for the typically sluggish reaction kinetics of the oxygen reduction reaction (ORR) at the cathode. When PEM fuel cells operate at temperatures above 100 °C, the product water will be present as vapor that can be more easily removed with the cathodic exhaust stream. Additionally, PEM fuel cell systems that can operate on dry gas feed streams are simpler because of the elimination of humidification and water

recovery subsystems. The most significant advantage of high-temperature operation, however, is the tolerance to fuel impurities. High temperature PEM devices based on a phosphoric acid-doped polybenzimidazole membranes have shown enhanced tolerance to fuel impurities, such as H_2S, CO, NH_3, and CH_3OH, as compared to low temperature PEMFCs.[2,7,8]

To increase the operating temperature of PEM fuel cells above 100 °C, researchers have investigated modified PFSA membranes, alternative thermally stable polymers, composites, and complexes of basic polymers with acids.[9] Acid-doped PBI membranes have received significant attention after Wainright et al. doped *m*-PBI films with phosphoric acid and demonstrated fuel cell operation of these membranes at temperatures of 100–200 °C.[10] PA-doped PBI membranes can be prepared by two processes: (1) conventional acid bath immersion and (2) a sol–gel process from a polyphosphoric acid solution. The resulting PA-doped *m*-PBI membranes (conventionally imbibed versus sol–gel) have been reported to have different macroscopic properties, such as ionic conductivity and mechanical integrity.[11]

In the conventionally imbibing process used to form PA-doped *m*-PBI membranes, a preformed dense polymer membrane is soaked in a concentrated phosphoric acid bath. The fabrication of conventionally imbibed PBI membranes involves an energy-intensive, multi-step process. *m*-PBI powder is dissolved in polar aprotic solvents, which sometimes contains dissolved salts, at high temperatures and pressures. This PBI solution is filtered and cast to form a membrane, which undergoes solvent evaporation, washing, and a final heat treatment. The preformed, dense PBI membrane is then immersed in an acid bath, which results in relatively low acid doping levels of 6–10 moles of PA per polymer repeat unit (PA/rpu) and moderate ionic conductivity for use in PEMFCs.[9] Several recent review articles summarize research and development efforts during the past 10 years that have focused on phosphoric acid-doped polybenzimidazole membranes.[2,4,12]

PA-doped PBI membranes were significantly advanced by the development of a sol–gel process, where the viscous polymerization solution of a PBI polymer dissolved in polyphosphoric acid is cast directly onto a substrate.[11] Upon exposure to atmospheric moisture, polyphosphoric acid is hydrolyzed to phosphoric acid. Phosphoric acid is a poor solvent for many PBIs compared to polyphosphoric acid. The change in solvent quality induces a transition from a viscous solution to a percolating gel network with good mechanical integrity. The ionic conductivities of sol–gel PA-doped PBI membranes were reported to be higher than 0.25S/cm[11] and the lifetimes, when used in high temperature PEM fuel cells at 160 °C, have exceeded 10,000 h.[13] As a result of their chemical and thermal stability, high ionic conductivity, and mechanical integrity, sol–gel PA-doped PBI membranes have been commercialized as proton exchange membranes for fuel cells in 10 W to 10 kW applications by BASF Fuel Cells.[12,14–16]

The literature contains limited findings regarding structure/property relationships in PA-doped PBI membranes. Research on the microstructure of PA-doped PBI membranes is mainly limited to PBI materials in the absence of phosphoric acid, the addition of which is essential for practical ionic conductivity.[17–23] These PBI studies have established the tendency of polybenzimidazole to form aggregates in solution.

In this work, a comparative study of PA-doped *m*-PBI membranes was conducted to investigate the structure and membrane properties that result from the two main processes used for membrane formation. The doping procedures and heat treatments were used to prepare *m*-PBI membranes with different levels of PA. The membrane compositions were determined before and after heat treatment to ensure accurate correlation between membrane compositions and the corresponding ionic conductivities and mechanical properties measured for the two types of membranes. Microstructural analyses were conducted via wide angle X-ray scattering (WAXS) and interpreted with the aid of atomistic simulations.

EXPERIMENTAL

Materials

m-PBI films (undoped, 55 μm thickness) were provided by BASF Fuel Cell GmbH. For the condensation polymerization of sol–gel processed PA-doped PBI membranes, 3,3′,4,4′-tetraaminobiphenyl (TAB, polymerization grade) provided by Celanese Ventures, GmbH and isophthalic acid (IA, 99+%) from Amoco were used without further purification. The polymerization solvent, polyphosphoric acid (115–116 wt %), was acquired from Aldrich and FMC Corporation. Equilibration baths of different concentrations were produced by dilution of 85 wt % *o*-phosphoric acid purchased from Fisher Scientific.

Membrane Preparation

PA-doped *m*-PBI membranes were prepared by two processes: conventional imbibing through immersion in acid baths and the sol–gel process. Conventionally imbibing of commercial *m*-PBI films was conducted by three separate washings in 70 °C distilled water followed immediately by soaking the films in 85 wt % *o*-phosphoric acid for 24 h at room temperature. In the sol–gel process, PA-doped *m*-PBI membranes were prepared by first polymerizing stoichiometric amounts of IA and TAB in polyphosphoric acid at 240 °C for 20 h with continuous stirring under nitrogen.[11] To adjust the solution viscosity prior to casting, the polyphosphoric acid solution was diluted with *o*-phosphoric acid and stirred for an additional 2 h. The solution, held at 240 °C, was cast onto a glass plate using a doctor blade (10–20 mm). Upon exposure to the laboratory atmosphere (30% RH at 21 °C) for 24 h, a solution-state to gel-state (sol–gel) transition was observed.

To adjust the PA content in the membranes, the PA-doped PBI membranes were equilibrated in phosphoric acid baths of different concentrations. After exposure to atmospheric moisture, the stable sol–gel PA-doped PBI membranes were equilibrated in 57 wt % PA baths at room temperature for

>16 h. A section of the sol–gel and the conventionally imbibed PA-doped *m*-PBI membranes were equilibrated in either a 72 or 31 wt % PA bath for an additional 16 h or longer. For the heat treatment study, sections of *m*-PBI membranes were heat treated for 5 days at 120 °C on Kapton support films in air.

Membrane Characterization

The PA-doped PBI membranes were characterized in terms of inherent viscosity, acid content, ionic conductivity, mechanical behavior, and structure using WAXS. For inherent viscosity measurements, crushed PBI polymer was neutralized with ammonium hydroxide, washed, and then vacuum dried at 110–130 °C overnight. The inherent viscosities (average error ± 0.03 dL/g) of approximately 0.2 g/dL solutions in 96% sulfuric acid were determined using a Cannon Ubbelohde viscometer at 30.0 °C.[11]

Compositions were determined before and after heat treatment. PA-doped PBI membranes from different PA baths were preweighed (W_{wet}) and then titrated with a 0.1 M sodium hydroxide (NaOH) solution using a Metrohm 716 DMS Titrino titrator. The titrated membranes were dried in a 110–130 °C oven for >8 h. The neutralized specimens were cooled in a vacuum and weighed to achieve a dry solids weight, W_{dry}. The average acid doping level, in moles of phosphoric acid per PBI repeat unit (PA/rpu), is determined from eq 1[11]:

$$\mathrm{PA/rpu} = \frac{(V_{NaOH} \cdot [NaOH])}{(W_{dry}/MW)}, \quad (1)$$

where the volume of sodium hydroxide is V_{NaOH} and the molecular weight of the polymer repeat unit is MW. The solids content (solids%) was determined before and after heat treatment by the ratio of dry weight to the initial wet weight, as in eq 2:[11]

$$\mathrm{Solids\%} = \frac{W_{dry}}{W_{wet}} \times 100. \quad (2)$$

Ionic conductivity data were obtained using a four-probe AC impedance method to investigate the bulk membrane conduction.[11] Rectangular pieces (3.5 × 7.0 cm^2) of PA-doped PBI membranes were loaded into a glass conductivity cell attached with four Pt wires. Current was supplied through the outer wires, while the potential difference was measured between the inner wires. The cell was attached to a Zahner IM6e spectrometer. The cell was heated in 20 °C increments to 180 °C in an oven open to the laboratory atmosphere with no humidity controlled equipment to simulate dry conditions.[11] The temperature was equilibrated for 10 min and four-probe impedance data (over a frequency range from 1 Hz to 100 kHz) was collected. The Nyquist plot of membrane resistance across the frequency range was fitted to a two-component model with an Ohmic resistor in parallel with a capacitor. Ionic conductivity, σ, was calculated from the following eq 3:

$$\sigma = \frac{d}{lwR}, \quad (3)$$

where the distance between the test electrode and sensor electrode (d) was 2.0 cm, which is divided by the product of the thickness (l), width (w), and membrane resistance (R). All data reported herein were obtained on a second heating cycle after the membrane was cooled in a vacuum. The thickness measurements used in the conductivity calculations were taken after the second heating cycle to account for shrinkage due mainly to water loss.

The stress–strain curves were acquired using an Instron Model 5843, equipped with a 10 N load cell and a non-contact type video extensometer, at a strain rate of 5 mm/min. The tensile measurements were performed on wet dumb-bell-shaped specimens cut to the ASTM standard D638 (Type V specimen) without environmental control. The dumb-bell-shaped specimens were cut perpendicular to the casting direction with a manual press equipped with a precision die. Five tensile tests were performed on each membrane with a particular acid doping level and processing treatment before and after heat treatment. The heat-treated membranes (and the conventional *m*-PBI membrane with 26 wt % solids and 7 PA/rpu) were held with sandpaper to prevent catastrophic slippage in the pneumatic grips. For registration of the video extensometer, two white dots (~20 mm apart) were painted on the membranes not more than 2 h before testing just outside of the gauge length (7.62 mm). The elastic modulus, yield point, and maximum stress were evaluated from the stress–strain curves. The elastic modulus was obtained from a linear regression of the steepest region of the curve before the yield point. The yield point was generally followed by strain hardening and a maximum stress value defined as the failure point. Yield point was defined as the intersection of the linear regression obtained for the modulus after shifting by 2% of the elongation at failure.

To investigate bulk ordering in the membranes as function of process, specimens with similar compositions were analyzed on a PANalytical X'Pert Pro instrument equipped with a Cu K_α X-ray target (at 45 kV and 40 mA) and a miniprop point detector with a parallel plate collimator from 2 to 40° 2θ over 1 h 45 min. The incident X-ray beam passes through a ½° fixed slit, a parabolic multilayer mirror, and 0.04 rad Soller slits. The diffracted X-ray beam is collected after passing through parallel plate collimator (0.09°) and 0.04 rad Soller slits. The benefit of these beam optics is that the incident X-ray beam is nearly monochromatic and "pseudo-parallel," which removes errors due to sample height variations.[24] WAXS scans with reflection and transmission geometries were collected using these beam optics.

WAXS scans were plotted with X'Pert HighScore Plus Version 2.2b software. The 1-D data using the mirror/parallel plate collimator/miniprop beam optics were fitted using ProFit Version 1.0c software. Background scans of the 1-D data in the reflection and transmission geometry were scaled to

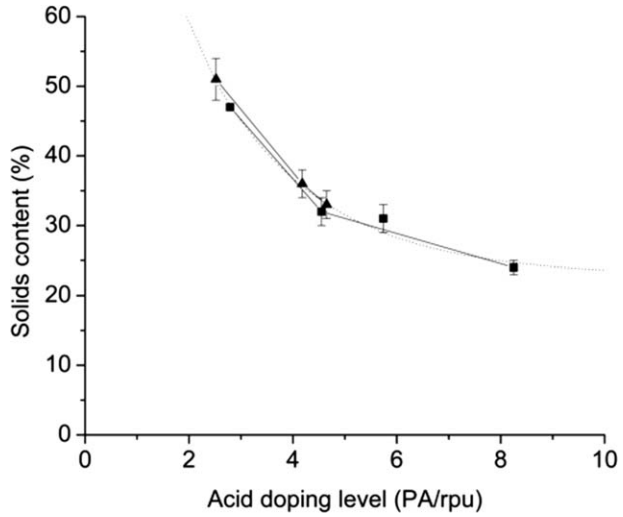

FIGURE 1 Correlation of solids content and acid doping level for heat-treated PA-doped *m*-PBI membranes for PA-doped *m*-PBI membranes prepared by the sol–gel process (-■-), conventional imbibing (-▲-), and exponential fit ($y = 0.2 + 0.9\ e^{-x/2.2}$) of the data (···).

correspond to the intensity at low angles ($<4^\circ$ 2θ) before subtraction. The scan was then individually fit using the ProFit software. For the 1-D data, the background was allowed to be refined by slope and intensity. First a wide, full-width at half-maximum (FWHM) = 10.38, peak was fit between 5 and 35° 2θ, allowing position, width, and intensity to be refined. After fixing what is termed the "amorphous halo," additional narrower (FWHM = 2) peaks were added and refined by position, width, and intensity. Then all peaks, including the amorphous halo, were refined. Additional peaks were added, if necessary. For the *m*-PBI membranes, the peak list from the most defined scan was then used to fit all the *m*-PBI scans. The FWHM for each peak, except the "amorphous halo," was reset to FWHM = 2 before refinement. The resulting fit agreed well with previous individual fits. Using this peak list, the bias of the experimentalist in determining how many peaks were present was removed. Three peaks related to sample holder and setup were found for both the conventional and sol–gel membranes from the WAXS studies. These peaks were relatively sharp with large spacings of 23.1, 15.4, and 11.7 Å that may result from clay, wax, or surfactant contaminants and due to their sharpness are not relevant for PA-doped PBI membrane interpretation.

To aid interpretation of the individual WAXS peaks, atomistic simulations (molecular mechanics) were performed on structural models of *m*-PBI using the MM3 Force-Field parameterization. A second energy minimization was performed after protonating the benzimidazole rings and adding phosphoric acid. From the second minimized structure, a classical molecular dynamics simulation was performed within the conical ensemble (500 K) for 5 ps followed by energy minimization, to simulate a thermal treatment.

RESULTS AND DISCUSSION

Acid Loading and Retention

PA-doped *m*-PBI membranes were prepared by conventional acid immersion (conventionally imbibed) and the sol–gel process, and then equilibrated in 31 and 72 wt % PA baths and heat-treated for 5 days at 120 °C. Figure 1 summarizes the solids content as a function of acid doping level after heat treatment. This demonstrates that the polymer-acid composition of the membranes scales in a similar manner for the two membrane fabrication processes. However, the sol–gel process is capable of producing membranes with overall higher PA contents (without excessive swelling, which could compromise the membrane integrity). The lower acid levels achieved by conventional imbibing techniques, even using PA baths of higher PA concentrations, demonstrate the inherent difficulties of doping (swelling) a dense preformed network, versus the relative ease of *in situ* PA doping through the sol–gel process.

Heat treatment of PA-doped *m*-PBI membranes at 120 °C reduced the water content as expected; however, partial reabsorption of water occurred during storage. This heat treatment would not be expected to affect phosphoric acid content because phosphoric acid has a relatively high boiling point. However, Figure 2 shows the change in acid doping level before and after heat treatment and indicates a reduction in acid doping level for all membranes after heat treatment most likely due to the ability of steam to remove some PA from the membrane. The final amount of PA in the membranes was similar for both membrane processes. The extrapolated line indicates that even at low doping levels, ~2 PA/rpu would remain in the membranes which corresponds with two phosphoric acid molecules that protonate the two benzimidazole rings in the polymer repeat unit.[10]

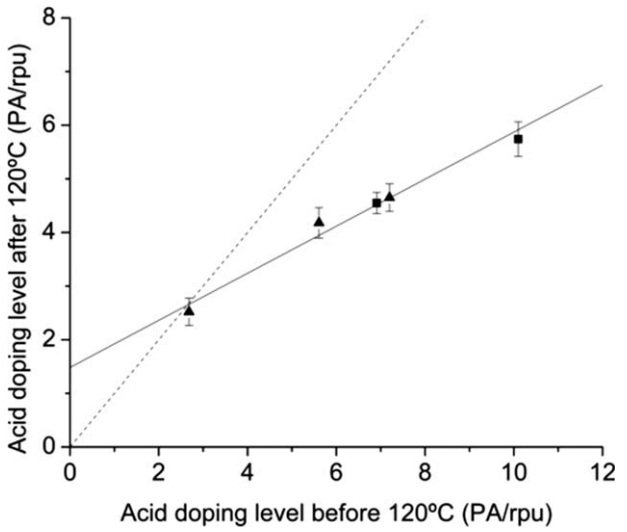

FIGURE 2 Acid doping level before and after heat treatment for sol–gel PA-doped *m*-PBI membranes (-■-) and conventionally imbibed membranes (-▲-). The dashed line indicates the line expected for no PA loss during heat treatment, and the solid line is the fitted line (linear regression) for the data.

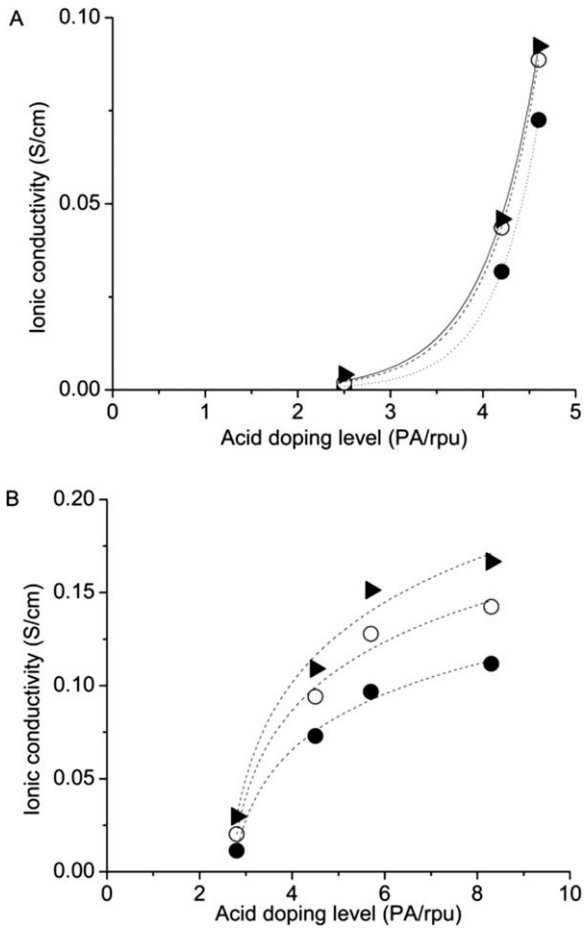

FIGURE 3 Effect of acid doping level on ionic conductivity for heat-treated (A) conventionally imbibed and (B) sol–gel *m*-PBI membranes at 120 °C (···●···), 140 °C (--○--), and 160 °C (-▶-). The error in acid doping level was ≤0.3 PA/rpu, except for the highest acid doping levels (8 ± 0.7 PA/rpu).

Ionic Conductivity

The ionic conductivity of PA-doped PBI membranes is related to the acid doping level, humidity, temperature, and pressure.[10] During an initial temperature increase to 180 °C in an open oven, the presence of "free water" (re-adsorbed) initially contributes to the ionic conductivity and yields higher ionic conductivity values.[25] After this initial dehydration of the adsorbed water, the ionic conductivity was slightly reduced and the dimerization of phosphoric acid to pyrophosphoric acid reaches an equlibrium.[26] This previous work noted that initial compositions of PA-doped PBI membranes are thus changed by this equilibrium after heat treatment. Therefore, membranes were first heat-treated and subsequent compositional analyses and ionic conductivities from the second heating cycle are presented.

The conductivity values at 120, 140, and 160 °C for different acid doping levels are shown in Figure 3 for heat treated (A) conventionally imbibed and (B) sol–gel PA-doped *m*-PBI membranes. Each process resulted in a clear difference in the relationships between ionic conductivity and acid doping level. Within this dataset that has minimal overlap in composition between the two processes, the conventional membranes with lower acid doping level exhibit an exponential relationship with proton conductivity, while the sol–gel membranes with higher acid doping level exhibit a logarithmic relationship. This limited dataset suggests that process and/or acid doping level leads to a change in the structure–property relationship of PA-doped PBI membranes. Within the region of compositional overlap, it was observed that membranes made by the sol–gel process had higher ionic conductivities than conventionally imbibed membranes at equivalent acid doping levels. As stated earlier, the sol–gel membranes retained high PA doping levels with equivalent doping and heat treatments, and thus are able to exhibit even higher ionic conductivities. The conventionally imbibed membranes in this study are simply unable to achieve such high acid doping levels and the associated ionic conductivities with equivalent treatments. From the conductivity curves shown in Figure 4 at similar acid doping levels (∼5 PA/rpu), the ionic conductivity of the heat-treated sol–gel PA-doped *m*-PBI was 6, 18, and 31% higher than the conventionally imbibed membrane at 140, 160, and 180 °C, respectively.

Note that the ionic conductivities measured for the conventionally imbibed PA-doped *m*-PBI membrane before and after heat treatment were higher than values previously reported (5 PA/rpu membrane: <0.03 S/cm at 150 °C and water activity between 0.1 and 0.25 P_{H_2O}/P_{sat}),[10] but are similar to those reported for conventional membranes with slight humidification (7 PA/rpu membrane: 0.09 S/cm at 170 °C and 10% RH).[10,25] As stated earlier, the only environmental control during the ionic conductivity tests reported in this article was temperature.

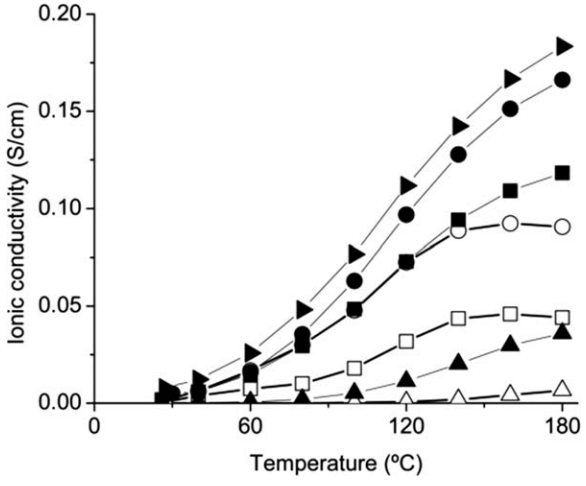

FIGURE 4 Ionic conductivities for heat-treated PA-doped *m*-PBI membranes at different acid doping levels for conventionally imbibed membranes [3 ± 0.3 (-Δ-), 4 ± 0.3 (-□-), and 5 ± 0.3 PA/rpu (-○-)] and sol–gel membranes [3 ± 0.2 (-▲-), 5 ± 0.2 (-■-), 6 ± 0.3 (-●-), and 8 ± 0.7 PA/rpu (-▶-)].

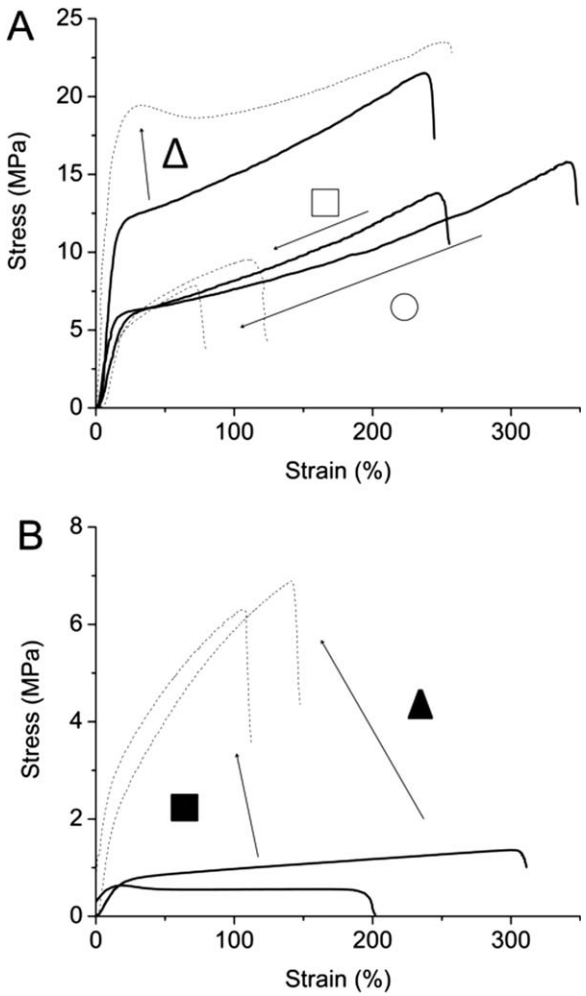

FIGURE 5 Stress–strain behavior of (A) conventionally imbibed and (B) sol–gel PA-doped *m*-PBI with different solids content before (bht) as a solid line and after (aht) heat treatment as a dash line at 120 °C. (A) Conventional membranes with 37 wt % solids content bht and 51 wt % aht (Δ), 29 wt % bht and 36 wt % aht (□), and 26 wt % bht and 33 wt % aht (○). (B) sol–gel membranes 22 wt % solids content bht and 32 wt % aht (▲), and 16 wt % bht and 31 wt % aht (■).

Mechanical Properties

The mechanical integrity of high temperature PEMs is essential for their long-term use in high temperature fuel cells and hydrogen pumps. To investigate the effect of solids content and acid doping level on mechanical properties, tensile testing was performed at ambient conditions on the conventional and sol–gel PA-doped *m*-PBI membranes before and after heat treatment.

The stress–strain behavior for the conventionally imbibed and sol–gel PA-doped *m*-PBI membranes before and after heat treatment is shown in Figure 5. The conventionally imbibed membranes before and after heat treatment exhibit well-defined yield points, while the yield point for the sol–gel membranes becomes significantly less pronounced after heat treatment. At solids content $\leq$29 wt % (acid doping level $\geq$6 PA/rpu), the conventionally imbibed membranes experienced a reduction in mechanical properties and ~50% loss in maximum stress after heat treatment. Conversely, for the PA-doped sol–gel *m*-PBI membranes, heat treatment increased the modulus, stress at yield point, and the maximum tensile stress. The heat-treated PA-doped *m*-PBI membranes (31–36 wt % solids) exhibited tensile strengths of <10 MPa and <150% elongation, and were quite similar for both membrane processes despite their differences prior to heat treatment. The conventionally imbibed membrane with much higher solids content (51 wt %) expectedly showed higher mechanical properties.

An inverse relationship was observed between membrane ionic conductivity that increased with increased acid content, and membrane mechanical properties that decreased with increased acid content. The membrane ionic conductivity and the stress at yield are plotted as a function of acid doping level in Figure 6. After heat treatment, conventional PA-doped *m*-PBI with ~5 PA/rpu and ~30 wt % solids content exhibited a stress at yield of 4 ± 0.6 MPa and an ionic conductivity 0.09 S/cm at 160 °C; similarly, a sol–gel PA-doped *m*-PBI membrane with a similar composition exhibited stress at yield of 3 ± 0.5 MPa and an ionic conductivity of 0.11 S/cm.

The sol–gel process membranes were able to attain acid doping levels not possible by conventional acid immersion. The sol–gel process provided membranes with higher ionic conductivity and somewhat lower mechanical properties, but still capable of being fabricated into membrane electrode assemblies suitable for fuel cell use.

Structural Analysis

The microstructure of proton exchange membranes is believed to contribute to the mechanical integrity, proton conductivity, and the ability to solvate protons.[27] WAXS permits the Å-scale characterization of bulk ordering in

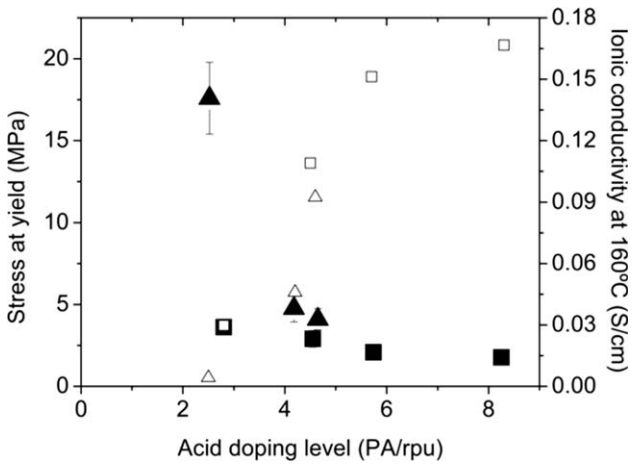

FIGURE 6 Effect of acid doping level on stress at yield (filled) and ionic conductivity at 160 °C (unfilled) for heat-treated conventionally imbibed (▲ and Δ) and sol–gel (■ and □) PA-doped *m*-PBI membranes.

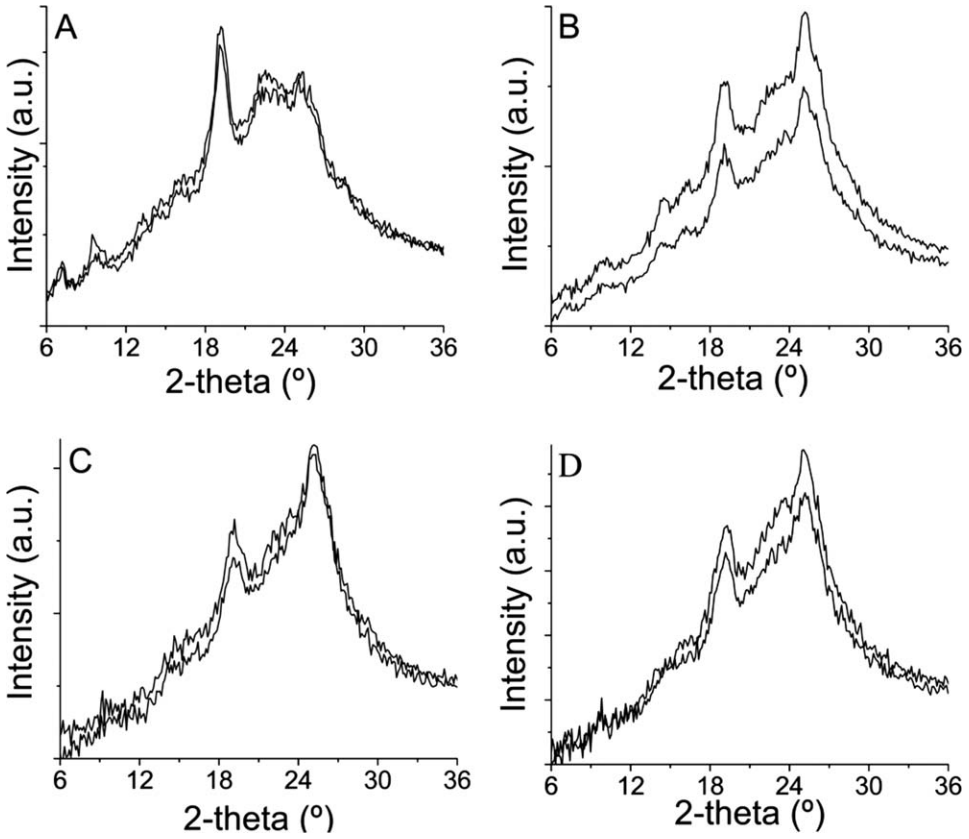

FIGURE 7 WAXS spectra of heat-treated (A and C) conventional (5 ± 0.3 PA/rpu and 33 ± 2 wt % solids) and (B and D) sol–gel (5 ± 0.2 PA/rpu and 32 ± 2 wt % solids) PA-doped *m*-PBI membranes. A and B are one-dimensional WAXS scans in reflection geometry taken parallel and perpendicular to the cast direction. C and D are one-dimensional WAXS scans in transmission geometry taken parallel and perpendicular to the cast direction.

polymers with minimal introduction of artifacts. Thus, WAXS was used to study conventionally imbibed and sol–gel PA-doped *m*-PBI membranes after heat treatment to elucidate differences in structural ordering.

To isolate the effects of process on properties, heat-treated PA-doped *m*-PBI membranes of similar composition were studied using WAXS with beam optics that reduced the error introduced by sample height, and thus permitted more accurate measurement of *d*-spacings. The heat-treated conventionally imbibed PA-doped *m*-PBI (5 ± 0.3 PA/rpu and 33 ± 2 wt % solids) that was equilibrated in 85 wt % phosphoric acid had essentially the same composition as the heat-treated sol–gel *m*-PBI membrane (5 ± 0.2 PA/rpu and 32 ± 2 wt % solids) equilibrated in 57 wt % phosphoric acid. WAXS patterns from heat-treated conventionally imbibed *m*-PBI membranes are shown in Figure 7(A, C), and the patterns from the sol–gel *m*-PBI membranes are shown for comparison in Figure 7(B, D), recorded in both the parallel and perpendicular directions relative to the membrane casting direction.

The peak positions observed in all the WAXS scans for PA-doped *m*-PBI membranes are similar; however, the intensities of the conventionally imbibed membrane appear to depend on direction, indicative of some degree of anisotropy. The predominant *d*-spacing parallel to the conventionally imbibed membrane surface is at $2\theta \sim 19^\circ$, yet the maximum intensity perpendicular to the membrane surface is at $2\theta \sim 25.5^\circ$. The sol–gel membrane is relatively isotropic; with a maximum intensity observed at $2\theta \sim 25.5^\circ$ for WAXS scans obtained both parallel and perpendicular to the sol–gel membrane surface.

A broad amorphous halo was observed in the WAXS patterns for both heat-treated conventionally imbibed and sol–gel PA-doped *m*-PBI membranes centered between $2\theta = 22$–24° with a FWHM = 9–14° as determined with peak fitting. In comparison, the other peaks identified in the WAXS patterns were narrower (FWHM = 0.4–3°). The two most intense peaks for both the heat-treated conventionally imbibed and sol–gel PA-doped *m*-PBI membranes were observed at $2\theta = 25.5 \pm 0.1$ and $19.1 \pm 0.1^\circ$, which corresponded to *d*-spacings 3.49 ± 0.02 and 4.63 ± 0.04 Å, respectively.

From peak fitting of the reflection and transmission geometry scans, the heat-treated sol–gel PA-doped *m*-PBI membranes exhibited nearly a 1:1 ratio of the peak intensities at $2\theta \sim 19$ and 25.5°. Conversely, the heat-treated conventionally imbibed PA-doped *m*-PBI membranes were anisotropic, as shown by the similar 1:1 ratio of peak intensities in the transmission scan versus the 2:1 ratio in the reflection scan.

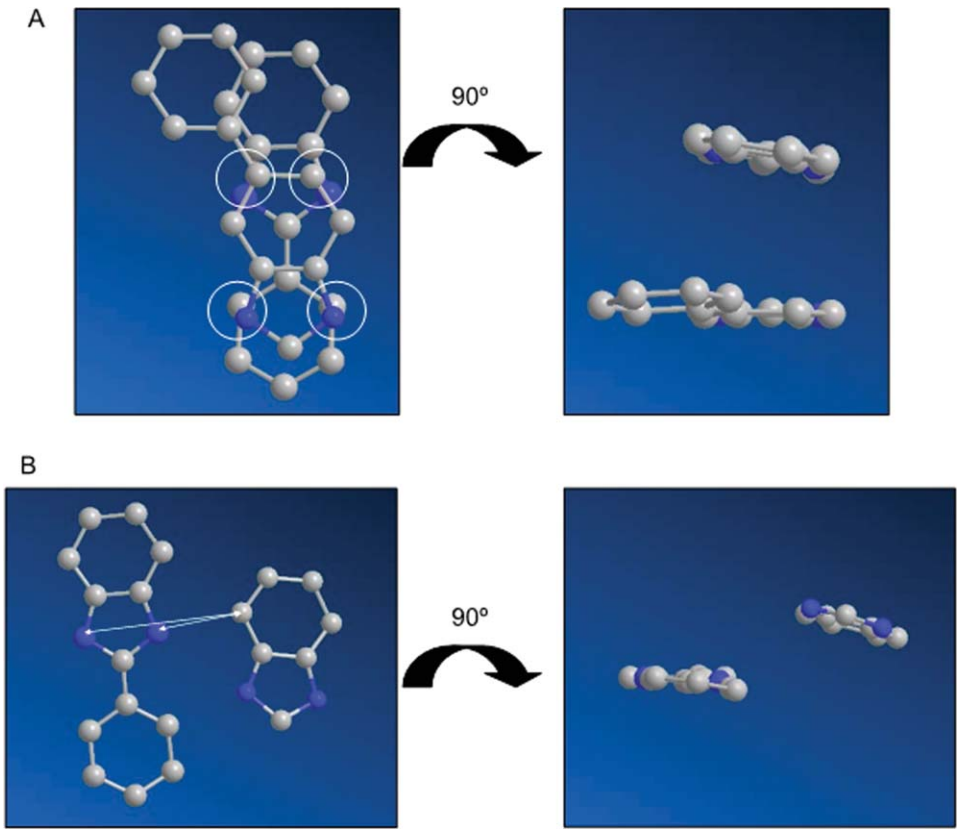

FIGURE 8 Environment within 6 Å of imidazole ring from classical atomistic simulations (molecular mechanics) illustrating (A) nearly perpendicular stacking (distance between atoms in circles in clockwise order: 3.74, 3.36, 3.71, and 3.33 Å) and (B) staggered side-to-side packing (distance between arrows 3.30 and 5.19 Å).

Therefore, the predominant *d*-spacing parallel to the conventionally imbibed membrane surface is 4.66 Å ($2\theta \sim 19^\circ$). Because of the relatively low intensity of the other WAXS peaks features that limits accurate peak fitting, interpretation focused on the more intense peaks that correspond to *d*-spacings of ~3.5 and 4.6 Å.

In poly(2,5-benzimidazole) films with and without acid, WAXS studies[28,29] observed ordering in the membranes consistent with a spacing of 3.3–3.5 Å, which was attributed to the stacking of the heterocyclic ring using the work by Berry on another rigid heterocyclic polymer.[30] WAXS studies of poly(bisbenzimidazobenzophenanthroline-dione) films found a reflection at 3.5 Å, which was identified as "repeat units stacked in a graphite-like array."[30] This published literature suggests that the 3.5 Å reflection observed in the WAXS data acquired from the heat-treated PA-doped *m*-PBI membranes is a result of stacking of the heterocyclic and/or phenyl ring of the polymer repeat unit. Additional published WAXS studies of poly(2,5-benzimidazole) also exhibited 3.3 Å, 4.2 Å, and wider spacings that were affected by phosphoric acid incorporation and mechanical stretching.[28]

To better interpret the structural contributions identified by the individual WAXS peaks, classical atomistic simulations (molecular mechanics) were performed on structural models of *m*-PBI in phosphoric acid using the MM3 Force-Field parameterization.[31,32] Eight protonated *m*-PBI chains in excess phosphoric acid underwent energy minimization and were subjected to a thermal treatment using molecular dynamics simulations at $T = 400$ K. From the simulations, the environments within 6 Å of the imidazole nitrogens were investigated. It was determined that 32 imidazole rings out of a total of 64, had a neighboring ring system within 6 Å. Of these 32 sets of imidazole rings, only 13 contained nearly parallel ring systems that corresponded with stacking or staggered side-to-side packing of the polymer chains.

For the parallel stacking, six examples of benzimidazole rings stacking with another ring system [an example is shown in Fig. 8(A)] were found and exhibited an average spacing of 3.42 ± 0.17 Å between the imidazole ring and the other ring system. Using experimental WAXS data acquired from heat-treated conventionally imbibed and sol–gel PA-doped *m*-PBI membranes, a *d*-spacing was identified of 3.49 ± 0.02 Å, which is in very good accord with the simulated spacing.

For the parallel staggered side-to-side packing, seven examples of benzimidazole rings exhibiting staggered side-to-side packing with no overlap of the imidazole ring with the benzimidazole or phenyl substituent of the neighboring polymer chain were identified. An example of staggered side-to-side

packing is shown in Figure 8(B). From the simulation, the average staggered side-to-side packing was 4.51 ± 0.27 Å. As discussed previously, the other predominant *d*-spacing in the WAXS data for heat-treated PA-doped *m*-PBI membranes was at 4.63 ± 0.04 Å, which is similar to the simulated staggered side-to-side packing.

To summarize for heat-treated PA-doped *m*-PBI, the predominant experimental WAXS *d*-spacings of 3.49 ± 0.02 and 4.63 ± 0.04 Å were interpreted as parallel ring stacking and staggered side-to-side packing with the support of atomistic simulations. In the published literature, other rigid-rod polymer systems, such as poly(*p*-phenylene benzobisthiazole), have exhibited "face-to-face" and "side-to-side" stacking of the heterocyclic rings with *d*-spacings of ~3.6 and 5.9 Å.[33] The ordering for *m*-PBI polymer in the presence of phosphoric acid appears to be consistent with literature trends of a narrower face-to-face stacking and a wider side-to-side packing. Also, the conventionally imbibed membranes exhibited an anisotropic scattering in the parallel and perpendicular directions which was not present in the sol–gel membranes.

CONCLUSIONS

PA-doped *m*-PBI membranes were prepared by two processes, conventional acid immersion (conventionally imbibed) and a sol–gel process. After equilibration in phosphoric acid baths, the sol–gel membranes were able to retain more acid than the conventionally imbibed membranes. Heat treatment at 120 °C caused a slight reduction in acid content of both the conventionally imbibed and sol–gel membranes. In general, the acid doping levels of sol–gel membranes were higher than conventionally imbibed membranes after heat treatment, demonstrating the ability of the sol–gel membrane to absorb and retain larger amounts of phosphoric acid at elevated temperatures when treated in an identical manner. As a result of the higher acid doping levels, sol–gel membranes exhibited higher ionic conductivity than conventionally imbibed membranes before and after heat treatment. The relationship between ionic conductivity and PA doping level exhibited fundamentally different behaviors over the range of doping levels examined in this study.

PA-doped *m*-PBI membranes having similar compositions were prepared from conventional immersion in 85 wt % PA and equilibration of sol–gel membranes in 57 wt % PA. At similar acid doping levels, the sol–gel membranes showed higher ionic conductivities than the conventionally imbibed membranes at the critical temperature range of 140–180 °C. WAXS studies of heat-treated PA-doped *m*-PBI membranes found slight anisotropy in the conventional membrane that was not present in the sol–gel membrane. Anisotropy of the conventional membranes was related to preferential side-to-side stacking of the ring systems parallel to the membrane surface. In addition, the conventional membranes with ≥6 PA/rpu lost significant mechanical performance with heat treatment and this loss in mechanical performance corresponded to an increase in the ordering identified predominantly at $2\theta = 19°$ ($d = 4.6$ Å) in the WAXS patterns. The anisotropic staggered side-to-side packing present in the conventional membranes may lead to a reduction in mechanical properties. Conversely, the sol–gel PA-doped *m*-PBI membrane exhibited enhanced mechanical properties and uniform ordering associated with $2\theta \sim 19$ and $2\theta \sim 25.5°$ 2θ ($d = 4.6$ and 3.5 Å) with heat treatment. In conclusion, PA-doped PBI membranes of the same polymer chemistry result in different structure–property relationships depending on process.

ACKNOWLEDGMENTS

This research was supported by ORNL's Shared Research Equipment (ShaRE) User Facility and Center for Nanophase Materials Science, which is sponsored by the Office of Basic Energy Sciences, U.S. Department of Energy. A portion of this work also was supported by DOE's Office of Fuel Cell Technologies, the NSF IGERT Fellowship Program, and the HERE Program at ORNL. Larry Walker and Shawn Reeves at ORNL are also acknowledged for their invaluable assistance.

REFERENCES AND NOTES

1 K. A. Perry, G. A. Eisman, B. C. Benicewicz, *J. Power Sources* **2008**, *177*, 478–484.

2 J. Mader, L. Xiao, T. J. Schmidt, B. C. Benicewicz, *Adv. Polym. Sci.* **2008**, *216*, 63–124.

3 J. A. Ansensio, E. M. Sánchez, P. Gómez-Romero, *Chem. Soc. Rev.* **2010**, *39*, 3210–3239.

4 Q. F. Li, J. O. Jensen, R. F. Savinell, N. J. Bjerrum, *Prog. Polym. Sci.* **2009**, *34*, 449–477.

5 B. S. Pivovar, W. H. Smyrl, E. L. Cussler, *J. Electrochem. Soc.* **2005**, *152*, A53–A60.

6 X. Yu, A. Roy, S. Dunn, A. S. Badami, J. Yang, A. S. Good, J. E. McGrath, *J. Polym. Sci. A* **2009**, *47*, 1038–1051.

7 Q. F. Li, R. H. He, J. A. Gao, J. O. Jensen, N. J. Bjerrum, *J. Electrochem. Soc.* **2003**, *150*, A1599–A1605.

8 T. J. Schmidt, J. Baurmeister, *ECS Trans.* **2006**, *3*, 861–869.

9 Q. F. Li, R. H. He, J. O. Jensen, N. J. Bjerrum, *Chem. Mater.* **2003**, *15*, 4896–4915.

10 J. S. Wainright, J. T. Wang, D. Weng, R. F. Savinell, M. Litt, *J. Electrochem. Soc.* **1995**, *142*, L121–L123.

11 L. X. Xiao, H. F. Zhang, E. Scanlon, L. S. Ramanathan, E. W. Choe, D. Rogers, T. Apple, B. C. Benicewicz, *Chem. Mater.* **2005**, *17*, 5328–5333.

12 D. C. Seel, B. C. Benicewicz, L. Xiao, T. J. Schmidt, In Handbook of Fuel Cells: Advances in Electrocatalysis, Materials, Diagnostics and Durability; W. Vielstich, H. A. Gasteiger, H. Yokikawa, Eds.; Wiley: Chichester, UK, **2009**; Vol. *5&6*, Chapter 19, pp 300–312.

13 S. Yu, L. Xiao, B. C. Benicewicz, In CARISMA Workshop on Ionomer Membranes for Medium and High Temperature Fuel Cells; Wiley-VCH Verlag Gmbh: Stuttgart, Germany, **2008**, pp 165–174.

14 M. Molleo, T. J. Schmidt, B. C. Benicewicz, In Encyclopedia of Sustainability Science and Technology; R. A. Meyers, Ed.; Springer Science + Business Media LLC: New York, **2012**.

15 T. J. Schmidt, *ECS Trans.* **2006**, *1*, 19–31.

16 T. J. Schmidt, J. Baurmeister, *ECS Trans.* **2008**, *16*, 263–270.

17 L. C. Sawyer, R. S. Jones, *J. Memb. Sci.* **1984**, *20*, 147–166.

18 T. S. Chung, C. M. Tun, K. P. Pramoda, R. Wang, *J. Memb. Sci.* **2001**, *193*, 123–128.

19 Y. H. Lu, J. M. Chen, H. X. Cui, H. D. Zhou, *Compos. Sci. Technol.* **2008**, *68*, 3278–3284.

20 A. Sannigrahi, D. Arunbabu, R. M. Sankar, T. Jana, *Macromolecules* **2007**, *40*, 2844–2851.

21 C. B. Shogbon, J. L. Brousseau, H. F. Zhang, B. C. Benicewicz, Y. A. Akpalu, *Macromolecules* **2006**, *39*, 9409–9418.

22 A. Sannigrahi, D. Arunbabu, T. Jana, *Macromol. Rapid Commun.* **2006**, *27*, 1962–1967.

23 D. Arunbabu, A. Sannigrahi, T. Jana, *J. Phys. Chem. B* **2008**, *112*, 5305–5310.

24 T. R. Watkins, O. B. Cavin, J. Bai, J. A. Chediak, In Advances in X-Ray Analysis; T. C. Huang, Ed; ICDD: Newtown Square, PA, **2003**; Vol. *46*, pp 119–129.

25 S. Yu, H. Zhang, L. Xiao, E.-W. Choe, B. C. Benicewicz, *Fuel Cells* **2009**, *9*, 318.

26 R. F. Savinell, J. S. Wainright, M. Litt, In Electrochemical Society Proceeding: Proton Conducting Membrane Fuel Cells (2nd International Symposium); S. Gottesfeld, T. F. Fuller, Eds; Fall: Boston, MA, **1998**; Vol. PV *98-27*, pp 81–90.

27 K. D. Kreuer, S. J. Paddison, E. Spohr, M. Schuster, *Chem. Rev.* **2004**, *104*, 4637–4678.

28 J. Cho, J. Blackwell, S. N. Chvalun, M. Litt, Y. Wang, *J. Polym. Sci., Part B: Polym. Phys.* **2004**, *42*, 2576–2585.

29 A. Wereta, M. T. Gehatia, D. R. Wiff, *Polym. Eng. Sci.* **1978**, *18*, 204–209.

30 G. C. Berry, *J. Polym. Sci. Polym. Phys. Ed.* **1976**, *14*, 451–478.

31 N. L. Allinger, Y. H. Yuh, J.-H. Lii, *J. Am. Chem. Soc.* **1989**, *111*, 8551–8565.

32 B. G. Sumpter, P. Kumar, A. Mehta, M. D. Barnes, W. A. Shelton, R. J. Harrison, *J. Phys. Chem. B* **2005**, *109*, 7671–7685.

33 H. H. Song, S. K. Hong, *Polymer* **1997**, *38*, 4241–4245.